Pramāṇa, Vol. 8, No. 2, 1977, pp. 184–204. © Printed in India.

A simple white beam neutron diffraction technique

A H VENKATESH and K R RAO
Nuclear Physics Division, Bhabha Atomic Research Centre, Bombay 400085

MS received 3 September 1976

Abstract. White beam neutron diffraction by time-of-flight (TOF) technique has been studied over a number of years as it is believed to be the most convenient method to investigate solids in a fixed geometry. This technique needs a pulsed neutron source and a suitable multichannel, analysing system. The entire system is in general, mechanically quite intricate and expensive.

We have investigated an alternative technique to achieve the end result of a constant geometry around the diffracting sample. This involves the use of a single crystal as an analyser to study diffraction pattern from the sample bathed in a white beam and diffracting at any fixed scattering angle. In this paper we report the results of our investigations and have compared this technique with other diffraction techniques. Taking Si, KCl and KNO_3 as typical specimens we have illustrated the results of our technique and we find that the results are comparable to those obtained by conventional neutron diffraction and TOF diffraction. The technique is simple in mechanical design and data acquisition. It can be easily adapted for high pressure diffraction which is being attempted.

Keywords. Neutrons; diffraction; technique.

1. Introduction

Conventional neutron diffraction makes use of a monochromatic beam technique as in x-ray diffraction. Figure 1 (*a*) illustrates the geometry. Usually a fixed wavelength λ ($\sim$ 1 Å) is chosen for the monochromatic beam and a BF_3 neutron detector is used for angular scan of diffracted intensity.

Due to the low reflectivity of most monochromators, the conventional diffraction technique is considered rather inefficient. Correlation techniques in which white beams are employed have been examined recently (Collwell *et al* 1968 and Gompf *et al* 1968). Sophisticated electronics and data processing are required for such measurements and the technique is not yet well established.

For single crystal neutron diffraction Hubbard *et al* (1972 and 1974) have demonstrated that white beam Laue diffraction [schematically shown in figure 1 (*b*)] is quite efficient.*

* A similar technique [*see* figure 1 (*c*)] for x-ray diffraction is normally referred to as x-ray energy dispersive technique and has been recently the subject of detailed investigation (Giesen and Gordon 1968, Cole 1970, Prabudha Banerjee and Paul Charbit 1971, Albritton and Malgrave 1972, Khadake 1973). This technique is gaining in importance in view of the active work on powder studies and use of synchrotron radiation.

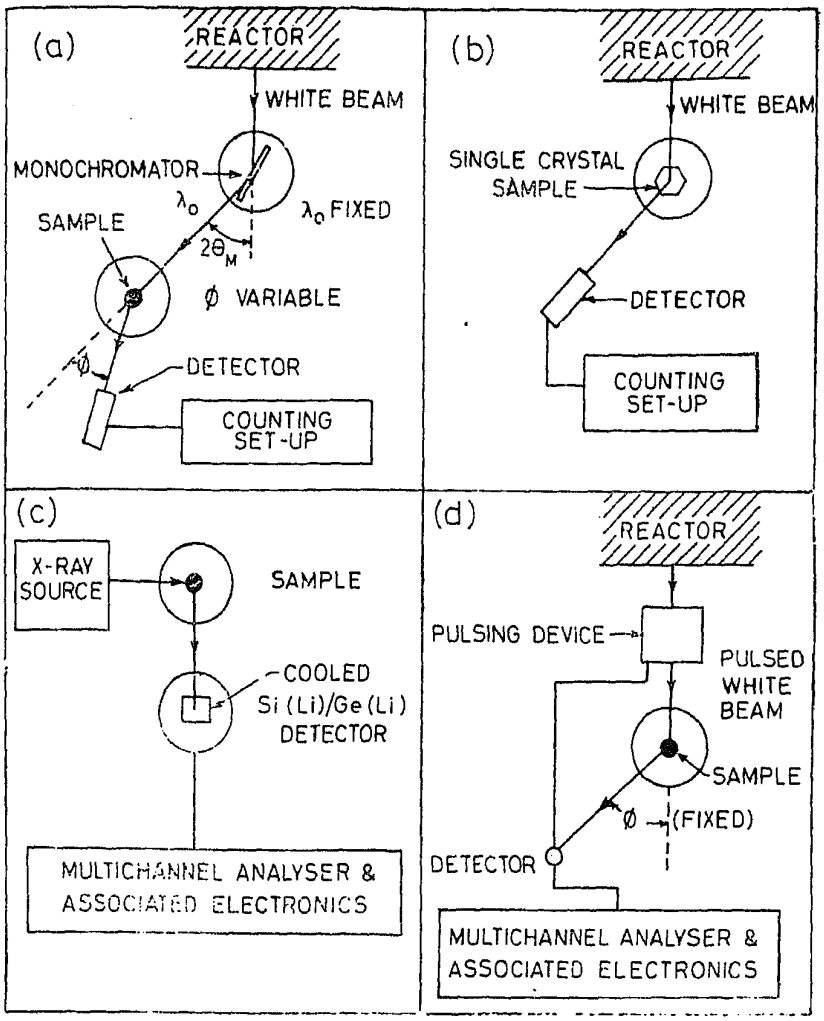

Figure 1. Different kinds of diffraction techniques currently used by experimentors; (*a*) conventional method for neutron diffraction-wavelength λ_0 is obtained from the whitebeam using a monochromator and diffraction pattern from the sample measured as a function of ϕ. (*b*) Laue streaks can be measured directly if the sample were a single crystal using white beam from reactor. Intensity of any streak is due to reflection from a certain (*hkl*) and its higher orders (*see* Hubbard *et al* 1972). (*c*) X-ray energy dispersive technique—incident energy spectrum is continuous (white) diffraction pattern at any angle is obtained by pulse height analysis using a solid; state detector. (*d*) Time-of-flight technique—neutrons in a narrow time-pulse travel over a long flight-path and get spread out in time; diffracted neutron components can be measured as a function of this time.

There are situations where one would find it difficult to move a detector around the sample and measure diffracted intensities. One example would be the study of diffraction from samples under externally applied pressure. A device in which a neutron beam is allowed to impinge on the sample through a narrow port and diffracted beam is observed at a fixed scattering angle through another port, is normally employed to hold the sample under pressure. Time-of-flight (TOF) white beam diffraction technique is suggested for this purpose. In this technique shown in figure 1 (*d*), the powder sample bathed in a collimated beam of polychromatic neutrons from the reactor diffracts the beam and the scattered neutrons are detected by a neutron detector at a suitable fixed scattering angle. The incident beam or sometimes the scattered beam is pulsed (using a mechanical chopper at a steady state reactor or by a pulsed reactor) and one records the TOF spectrum using the detector, Since the incident spectrum is white with varying wavelengths

and the scattering angle is fixed, the role of wavelength and scattering angle may be said to be reversed as compared to that in the conventional diffraction technique. The TOF technique has been tried out in several laboratories (Brugger 1965, Brugger *et al* 1969; Buras *et al* 1970, Buras 1975). As in the case of correlation techniques one relies on sophisticated electronics and sophisticated pulsing devices. Its efficiency is not better than that of monochromatic diffraction due to the low duty cycle of the chopping system. However, this technique is most suited for a pulsed reactor where higher efficiency can be attained.

2. The present technique

One can meet the requirements of a constant scattering angle geometry for neutron diffraction by a technique recently studied by us. Although this technique is very simple in principle, it has not so far been studied or applied. Figure 2 (*a*) shows this technique. A white beam of neutrons from the reactor falls on the sample and the diffracted beam is observed at a fixed scattering angle. The scattered beam is wavelength-analysed using an analysing single crystal and a BF_3 detector. The efficiency of the system for powder studies is found comparable to that of conventional diffraction. Its advantage over the conventional technique is that one can study samples at a fixed scattering angle as in the TOF method. Its advantage over the TOF method is that no pulsing device or sophisticated electronics are required.

We have adopted a triple axis neutron spectrometer for these studies. The triple axis spectrometer has, as the name suggests, three axes on which are mounted a monochromator, the sample and an analyser (Iyengar 1965, Rao 1968). We

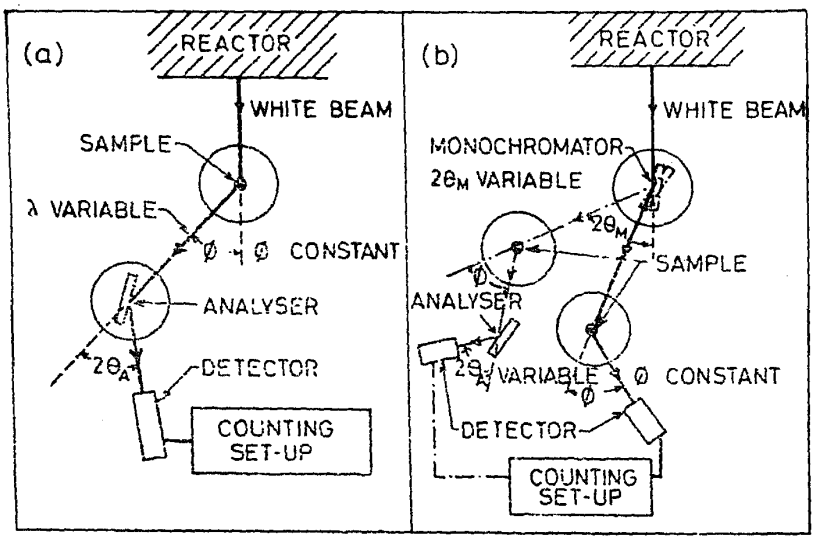

Figure 2. (*a*). The white beam neutron diffraction technique investigated by us is shown in (*a*). The white beam from the reactor gets diffracted by the specimen and observed at a fixed scattering angle. Intensities due to various (*hkl*) reflections are analysed using a single crystal as an analyser by sweeping the analyser detector in a $\theta_A - 2\theta_A$ mode (*b*) A method recently used by Buras *et al* (1973). On the left in this part of the diagram is shown the method where elastic diffraction technique is employed using a triple axis spectrometer. On the right the same instrument is used in the standard diffraction mode, but instead of varying ϕ at sample, one varies $2\theta_M$.

have chosen to mount the sample on the table normally used for the monochromating crystal and the analyser is mounted on the table normally used for the sample [see figure 2 (*a*)]. One can choose any scattering angle at the sample permitted by the first axis and its paraphernalia and scan diffracted beam intensities due to various (*hkl*)s of the sample at this chosen angle using the analyser and the detector in the $\theta_A - 2\theta_A$ combination. The scheme has the advantage that a suitably designed high pressure device can be mounted on the first axis inside the monochromating drum. The drum provides adequate shield around the high pressure device against any accidental ruptures.

In this method high intensities with high contrast are achieved by proper selection of the scattering angle. Contrast is obtained by increasing $\triangle\lambda/\triangle d$ where the ratio is the change in wavelength per unit change in the interplanar spacing. Since

$$\lambda = 2d \sin\theta$$

$$\triangle\lambda/\triangle d = 2 \sin\theta = 2 \sin(\phi/2). \tag{1}$$

Therefore high scattering angles are favoured for increasing contrast. However, intensity favours low scattering angles [see eq. (24)]. Hence a suitable compromise has to be made between contrast and intensity. One should also consider the equation

$$\lambda = 2d_{hkl} \sin\theta = 2d_A \sin\theta_A \tag{2}$$

which defines the analyser angle θ_A where λ is observed. Here d_A is the interplanar spacing of the analyser used for analysis of the scattered wavelength distribution. The white spectrum-weighted analyser-detector efficiency is low for $\theta_A < \theta_{A,\min}$ and $\theta_A > \theta_{A,\max}$ (we may consider the efficiency to be low if it is less than say one per cent of its maximum value). Hence the choice of scattering angle has to be such that reflection from (*hkl*) is observable in the range $\theta_{A,\min}$ to $\theta_{A,\max}$ of the analyser Bragg angle.*

3. Intensity and resolution of the technique

The effect of beam divergences and scattering angle on the intensity and full-widths at half-maximum (FWHM) can be discussed following the method of Caglioti *et al* (1958). We shall retain their arguments wherever applicable and analyse the present technique. The plan of the analysis is that (*a*) the path of an individual neutron is traced, (*b*) probabilities for the neutron to reach the detector through various elements along the path like the collimators, the sample and the analyser are assigned and (*c*) the probabilities are summed over various paths acceptable by the parameters of the system. In considering collimation effects

* We have recently learnt that Buras (1975) have also used a triple axis spectrometer for diffraction at a fixed scattering angle for high pressure application. They mounted a high pressure device containing a sample on the sample table and observed the diffraction pattern by varying the monochromator settings continuously with or without an analyser, keeping the scattering angle fixed [figure 2 (*b*)]. Further details of their work are not available from the point of view of relative assessments, etc. It may be mentioned that in our laboratory the same technique has been used over a number of years for calibrating the filter detector spectrometer which also has a monochromator whose settings can be varied and a sample table to mount the specimens for study.

we shall take into account only the horizontal collimation. Since the vertical collimation is generally much relaxed in collimators of neutron spectrometers this will lead to second order effects on resolution and intensity. Secondly we make use of the Gaussian approximation for neutron transmission through a collimator. In the following derivation, therefore, we assume that (i) the vertical collimation is relaxed, (ii) the variation of extinction with wavelength in sample and analyser can be neglected, and (iii) the width ($\triangle\lambda$) of any reflection is small, *i.e.*, $\triangle\lambda \ll \lambda$.

The constant scattering angle $\phi\,(=2\theta_0)$ at the sample is determined by the centre lines of collimators Nos. 1 and 2 (*see* figure 3). Corresponding to the reflection (*hkl*), neutrons of wavelength λ_0 are given by

$$\lambda_0 = 2d_{hkl} \sin\theta_0 \tag{3}$$

incident parallel to centre line of collimator No. 1 get Bragg reflected and pass through collimator No. 2 with maximum transmission probability. Consider neutrons of wavelength $\lambda\,(\neq \lambda_0$, in general) given by

$$\lambda = 2d_{hkl} \sin\theta \tag{4}$$

incident on the sample at an angle ψ_1 with the direction of the most probable neutron. The probability of these neutrons to pass through collimator No. 1 is

$$P_1 = \exp\{-(\psi_1/\alpha_1')^2\}$$

where

$$\alpha'_1 = \frac{\alpha_1}{2\sqrt{\ln 2}} \tag{5}$$

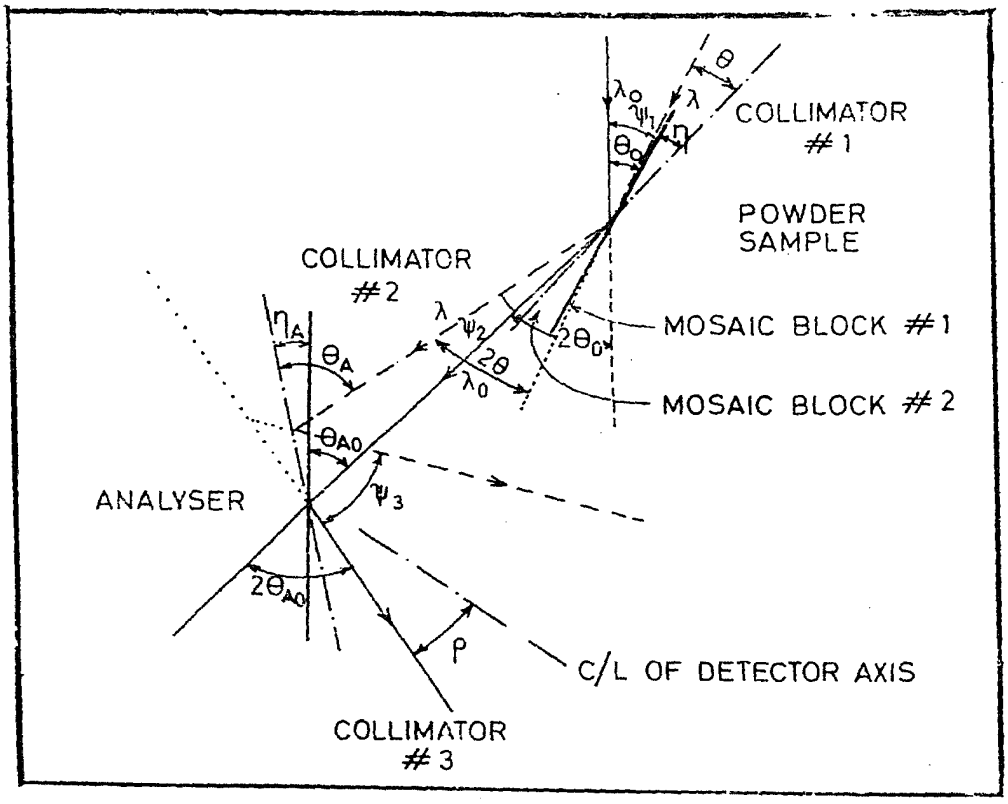

Figure 3. Detailed geometry of white beam diffraction. Expressions for intensity and resolution of the technique are derived using the various angular parameters occurring in this diagram. Note $\psi_1 < 0$ and $\eta > 0$ in this diagram.

a_1 being the FWHM of the collimator transmission function. These neutrons get Bragg scattered through angle ϕ [$= 2\theta$] [eq. (4)] from a micro-crystal block of the sample and pass through collimator No. 2 at an angle ψ_2 with respect to its centre line. The intensity scattered by the micro-block is

$$I_s \propto \frac{i(\lambda)\,\lambda^4 \mid F(hkl) \mid^2}{2\sin^2\theta} \frac{\triangle V}{V_c^2} A(\lambda) \tag{6}$$

where $i(\lambda)$ is the incident Maxwellian spectrum of neutron wavelengths, $\mid F(hkl) \mid^2$, the structure factor of (hkl) reflection in the sample, $\triangle V$, volume of the micro-crystal; V_c, volume of a unit cell; $A(\lambda)$, the absorpton factor in the sample.

The intensity scattered by the powder sample is given by multiplying the expression in eq. (6) by the number of (hkl) planes oriented between η and $\eta + \triangle\eta$, *viz.*,

$$\tfrac{1}{2}\cos\theta_0 j_{hkl} \frac{V}{\triangle V} d\eta \tag{7}$$

where j_{hkl} is the multiplicity of (hkl) reflection and $V/\triangle V$ the number of micro-crystals in the sample. If the difference in the Bragg angles is defined by

$$\delta = (\theta - \theta_0) \tag{8 a}$$

and η is the angle between the micro-blocks reflecting neutrons of wavelengths λ and λ_0 then the following relations hold:*

$$\eta = (\delta - \psi_1) \tag{8 b}$$

$$\psi_2 = (2\delta - \psi_1). \tag{8 c}$$

Thus the probability of neutrons of wavelength λ to be Bragg scattered from (hkl) planes of the sample is

$$P_s \propto \frac{i(\lambda)\,\lambda^4 \mid F(hkl) \mid^2 \triangle V A(\lambda)}{2\sin^2\theta\, V_c^2} \tfrac{1}{2}\cos\theta_0\, j_{hkl} \frac{V}{\triangle V} d\eta$$

$$\simeq \frac{i(\lambda_0)\,\lambda_0^4 \mid F(hkl) \mid^2}{4\sin^2\theta_0} \frac{V}{V_c^2} A(\lambda_0) \cos\theta_0 j_{hkl}\, d\eta. \tag{9}$$

The approximation involved in arriving at eq. (9) assumes that the probability of neutrons getting Bragg scattered does not vary within a reflection. The probability of the neutrons getting through collimator No. 2 is

$$P_2 = \exp\{-(\psi_2/\alpha'_2)^2\}$$

where

$$\alpha'_2 = \frac{a_2}{2\sqrt{\ln 2}}. \tag{10}$$

The experimental scan of (hkl) reflection is made by varying the analyser scattering angle $2\theta_A$ through the required range. When $2\theta_A$ equals $2\theta_{A_0}$ given by

$$\lambda_0 = 2d_A \sin\theta_{A_0} \tag{11}$$

* ψ_1 and η are taken to be positive if increase in either of them increases θ.

the analyser planes are at the correct orientation to diffract neutrons of wavelength λ_0 with maximum reflectivity (probability). This gives us the peak position of (hkl) reflection. At this point of the scan the neutrons of wavelength λ get diffracted through angle $2\theta_A$ by a mosaic block in the analyser which is at an angle η_A with respect to the block diffracting neutrons of wavelength λ_0. $2\theta_A$ is given by

$$\lambda_0 = 2d_A \sin\theta_A. \tag{12}$$

The angle ψ_3 between the trajectories of neutrons of wavelengths λ_0 and λ after diffraction from the analyser is given by

$$\psi_3 = 2\delta_A - 2\delta + \psi_1 \tag{13}$$

where

$$\delta_A = \theta_A - \theta_{A_0} \tag{14}$$

is the variation in analyser Bragg angle. If δ and δ_A are small, they are related by the equation

$$\delta_A = \delta a \tag{15}$$

where a is the ratio of dispersion at the sample to that at the analyser given by

$$a = \frac{\left(\frac{d\lambda}{d\theta}\right)_s}{\left(\frac{d\lambda}{d\theta}\right)_A} = \frac{d_{hkl}\cos\theta_0}{d_A\cos\theta_{A_0}}. \tag{16}$$

As we scan the reflection by varying the analyser Bragg angle the neutron trajectory remains unaltered; but its probability of reaching the detector changes because both the detector and the crystal analyser have been rotated. Suppose the detector axis has been rotated through an angle ρ away from the peak position, *i.e.*, the analyser scattering angle now is $(2\theta_{A_0} + \rho)$. (It should be recalled here that the crystal analyser itself is rotated through half the angle $(\rho/2)$ in the proper direction so as to ensure that the Bragg condition is favoured.) Neutrons of wavelength λ now get diffracted by a block in the analyser which is at an angle $(\eta_A - \rho/2)$ with respect to the most probable block. Moreover these neutrons go through the collimator No. 3 at an angle $(\psi_3 - \rho)$ with respect to its centre line. Thus the probabilities for the neutrons of wavelength λ to be diffracted by the analyser and to go through the collimator No. 3 are respectively given by P_A and P_3:

$$P_A \propto R(\lambda)\exp\left\{-\left(\frac{\eta_A - \rho/2}{\beta'_A}\right)^2\right\} d\eta_A$$

where

$$\beta'_A = \frac{\beta_A}{2\sqrt{\ln 2}}, \tag{17}$$

$R(\lambda)$ is the reflectivity of the crystal and β_A the FWHM of analyser mosaic distribution assumed to be a Gaussian and

$$P_3 = \exp\left\{-\left(\frac{\psi_3 - \rho}{\alpha'_3}\right)^2\right\} \tag{18}$$

where

$$\alpha'_3 = \frac{\alpha_3}{2\sqrt{\ln 2}},$$

α_3 being the horizontal parameter for collimator No. 3. As before, if the width $\Delta\lambda$ is small, P_A may be approximated to

$$P_A \propto R(\lambda_0) \exp\left\{ -\left(\frac{\eta_A - \rho/2}{\beta'_A}\right)^2 \right\} d\eta_A \tag{19}$$

η_A is related to ψ_1 and δ through the equation

$$\eta_A = \delta(a-2) + \psi_1. \tag{20}$$

Thus the total probability for neutrons of wavelength λ to reach the detector is given by the product of eqs (5), (9), (10), (18) and (19). The probability $J(\rho, \psi_1, \delta)\, d\rho\, d\psi_1\, d\delta$ for a neutron to go through collimator No. 1 making an angle $(\psi_1, \psi_1 + \Delta\psi_1)$ with respect to its centre line, to get Bragg scattered by the (hkl) planes of the powder sample with the angle $(\delta, \delta + \Delta\delta)$, to pass through collimator No. 2 to get Bragg scattered by the analyser planes and then finally to reach the detector whose axis makes an angle $(\rho, \rho + \Delta\rho)$ with the direction $2\theta_{A_0}$ through collimator No. 3 is given by

$$J(\rho, \psi_1, \delta)\, d\rho\, d\psi_1\, d\delta \propto \left\{ \exp -\left[\left(\frac{\psi_1}{\alpha'_1}\right)^2 + \left(\frac{\psi_2}{\alpha'_2}\right)^2 + \left(\frac{\eta_A - \rho/2}{\beta'_A}\right)^2 + \left(\frac{\psi_3 - \rho}{\alpha'_3}\right)^2 \right] \right\} d\rho\, d\psi_1\, d\delta. \tag{21}$$

The number of neutrons detected by the detector with an efficiency $\chi(\lambda_0)$ at the detector angle $(\rho, \rho + \Delta\rho)$ is given by

$$J(\rho)\, d\rho \propto \chi(\lambda_0) \{ \int\int J(\rho, \psi_1, \delta)\, d\psi_1\, d\delta \}\, d\rho$$

$$= H \{ \int_{-\infty}^{\infty} \int_{-\infty}^{\infty} \exp[-(4 \ln 2) F(\psi_1, \delta, \rho, a)]\, d\psi_1\, d\delta \}\, d\rho \tag{22}$$

where

$$F(\psi_1, \delta, \rho, a) = \left(\frac{\psi_1}{\alpha_1}\right)^2 + \left(\frac{2\delta - \psi_1}{\alpha_2}\right)^2 + \left(\frac{\psi_1 - \delta(2-a) - \rho/2}{\beta_A}\right)^2 + \left(\frac{\psi_1 - \rho - 2\delta(1-a)}{\alpha_3}\right)^2 = l^2 \psi_1^2 + m^2 \delta^2 + n^2 \rho^2 + 2p\psi_1\delta + 2q\psi_1\rho + 2r\rho\delta \tag{23}$$

and

$$H \propto \frac{\lambda_0^4 |F(hkl)|^2 \cos\theta_0}{\sin^2\theta_0} i(\lambda_0) R(\lambda_0) \chi(\lambda_0) A(\lambda_0). \tag{24}$$

Here

$$l^2 = \frac{1}{\alpha_1^2} + \frac{1}{\alpha_2^2} + \frac{1}{\beta_A^2} + \frac{1}{\alpha_3^2}$$

$$m^2 = \frac{4}{\alpha_2^2} + \frac{(2-a)^2}{\beta_A^2} + \frac{4(1-a)^2}{\alpha_3^2}$$

$$n^2 = \frac{1}{4\beta_A^2} + \frac{1}{a_3^2}$$

$$2p = -\frac{4}{a_2^2} - \frac{2(2-a)}{\beta_A^2} - \frac{4(1-a)}{a_3^2}$$

$$2q = -\frac{1}{\beta_A^2} - \frac{2}{a_3^2}$$

$$2r = \frac{(2-a)}{\beta_A^2} + \frac{4(1-a)}{a_3^2}. \tag{25}$$

We use the identity,

$$\int_{-\infty}^{\infty} \exp(-px^2 \pm qx)\, dx = \sqrt{\frac{\pi}{p}} \exp\left(\frac{q^2}{4p}\right) \tag{26}$$

twice to obtain

$$I(\rho)\, d\rho = H \frac{\pi}{4 \ln 2} \frac{}{\sqrt{m^2 l^2 - p}} \exp\left\{-4 \ln 2 \left(n^2 - \frac{q^2}{l^2} - \frac{(rl^2 - qp)^2}{l^2 (ml^2 - p^2)}\right) \rho^2\right\} d\rho$$

$$= H \frac{\pi}{4 \ln 2} \frac{a_1 a_2 a_3 \beta_A}{\gamma} \exp\left\{-4 \ln 2 \frac{(a_2^2 + a_3^2 + 4\beta_A^2)}{\gamma^2} \rho^2\right\} d\rho \tag{27}$$

where

$$\gamma^2 = [4(a_2^2 a_3^2 + a_2^2 \beta_A^2 + a_3^2 \beta_A^2) - 4a a_2^2 (a_3^2 + 2\beta_A) + a^2 \{a_1^2 a_2^2 + a_2^2 a_3^2 + a_3^2 a_1^2 + 4\beta_A^2 (a_1^2 + a_2^2)\}]. \tag{28}$$

The FWHM of this intensity distribution is,

$$(2\delta_A) = \frac{\gamma}{\sqrt{(a_2^2 + a_3^2 + 4\beta_A^2)}}. \tag{29}$$

The peak intensity and integrated intensity are given by

$$I_{\text{peak}} = H\left(\frac{\pi}{4 \ln 2}\right) \frac{a_1 a_2 a_3 \beta_A}{\gamma} \tag{30}$$

and

$$I = \int I(\rho)\, d\rho = H \sqrt{\left(\frac{\pi}{4 \ln 2}\right)^3} \frac{a_1 a_2 a_3 \beta_A}{\sqrt{a_2^2 + a_3^2 + 4\beta_A^2}} \tag{31}$$

4. Results

The purpose of the study has been to assess the technique using a few samples and standard crystal analysers and compare our results with that from other white beam techniques wherever possible. Silicon has been studied well by TOF diffraction technique by Buras *et al* (1964). KCl has been studied by x-ray energy dispersive technique (Prabudha Banerjee and Paul Charbit 1971). KNO_3 has been studied using TOF technique by Brugger *et al* (1965) at various pressures. Hence,

we have chosen these samples to compare the data by our technique with those obtainable by other methods. We have used Cu (200), Be ($11\bar{2}0$) and Ge(111) analysers. Cu (200) and Be ($11\bar{2}0$) are standard analysers, beryllium known for its small interplanar spacing and high reflectivity for neutrons. Ge (111) is chosen because of the absence of its second order reflection and its large interplanar spacing.

While comparing the calculated and measured intensities of diffraction peaks one has to apply several corrections and make some approximations. In presenting the results, however, we show the raw spectra measured through figures 5, 6 and 7.

From eq. (31) and eq. (24) we note that the integrated intensity for any (hkl) is given by

$$I(hkl) = K \frac{\lambda_0^4 \mid F(hkl) \mid^2 \cos\theta_0}{\sin^2\theta_0} \sqrt{\left(\frac{\pi}{4 \ln 2}\right)^3} \frac{\alpha_1\alpha_2\alpha_3\beta_A}{\sqrt{\alpha_2^2 + \alpha_3^2 + 4\beta_A^2}} \times i(\lambda_0)\, R(\lambda_0)\, \chi(\lambda_0)\, A(\lambda_0), \tag{32}$$

K being a proportionality constant.

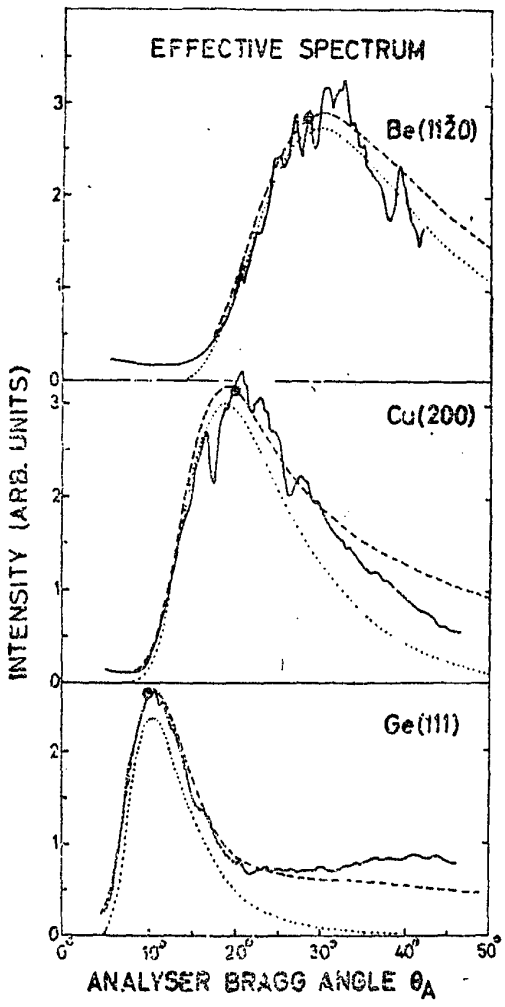

Figure 4. Spectra as measured using an incoherent sample. Intensity measured at any analyser angle is proportional to $\Sigma i(\lambda_0) R(\lambda_0) \chi(\lambda_0)$ where $i(\lambda_0)$ is the incident flux, $R(\lambda_0)$ the reflectivity of the analyser and $\chi(\lambda_0)$ efficiency of the detector. The peaks and valleys in the effective spectrum are due to multiple Bragg effects in the analyser. Assuming a Maxwellian incident neutron spectrum one can calculate the overall effective spectrum. Results of calculations are shown by dashed lines (normalised at the point marked by ⊗). Dotted lines indicated I order contributions only.

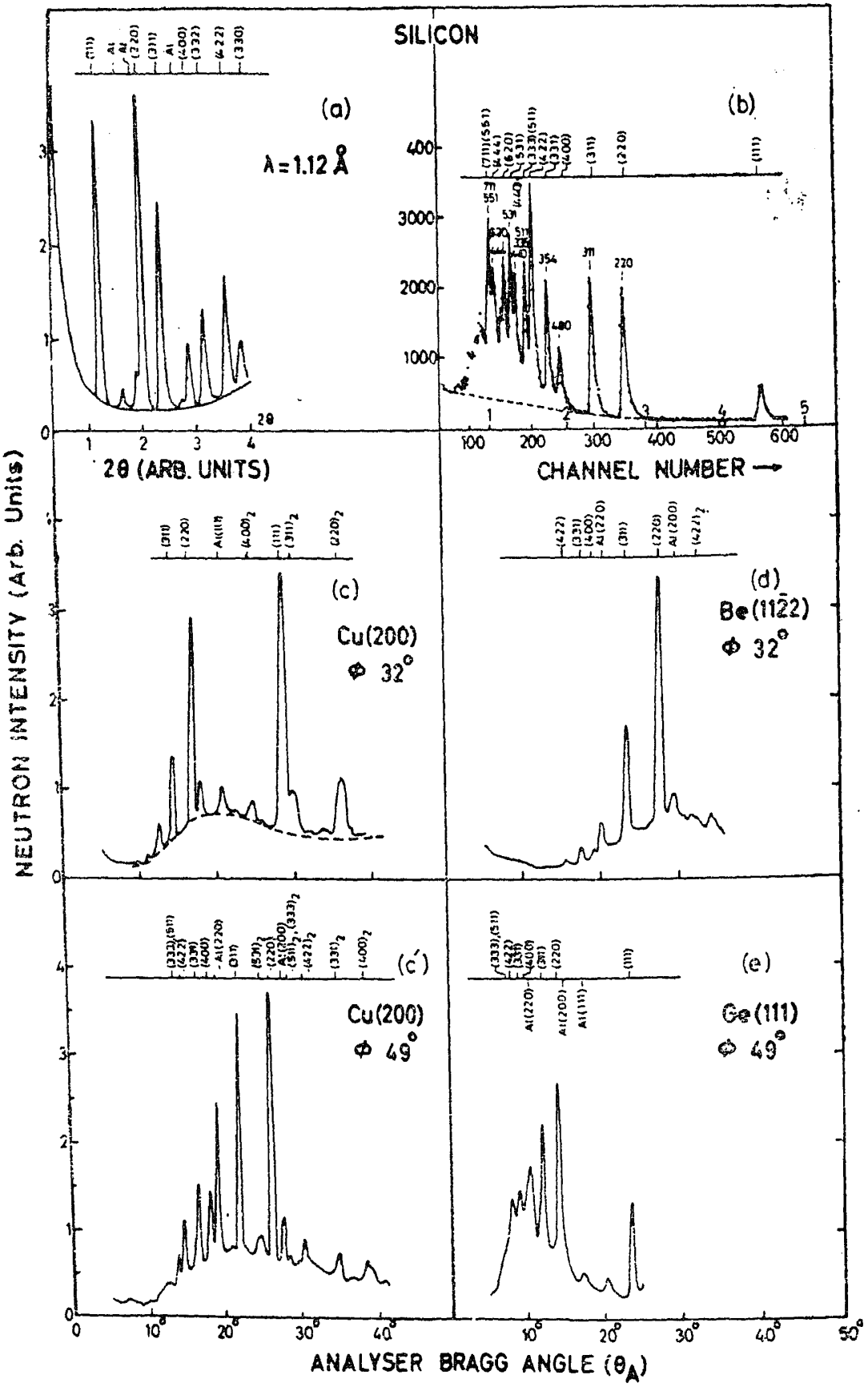

Figure 5. Comparison of results in case of silicon using different techniques: (*a*) diffraction pattern by conventional method (Buras *et al* 1964), (*b*) diffraction pattern by TOF technique (Buras *et al* 1964), (*c*) through (*d′*) indicate results by the present technique, using Cu (200), Be (11$\bar{2}$0) and Ge (111) analysers. The dashed line in (*c*) indicates the estimated background. Similar backgrounds are taken into account in arriving at integrated intensities. Indices $(hkl)_2$ correspond to (hkl) reflection of the sample observed through the second order in the analyser.

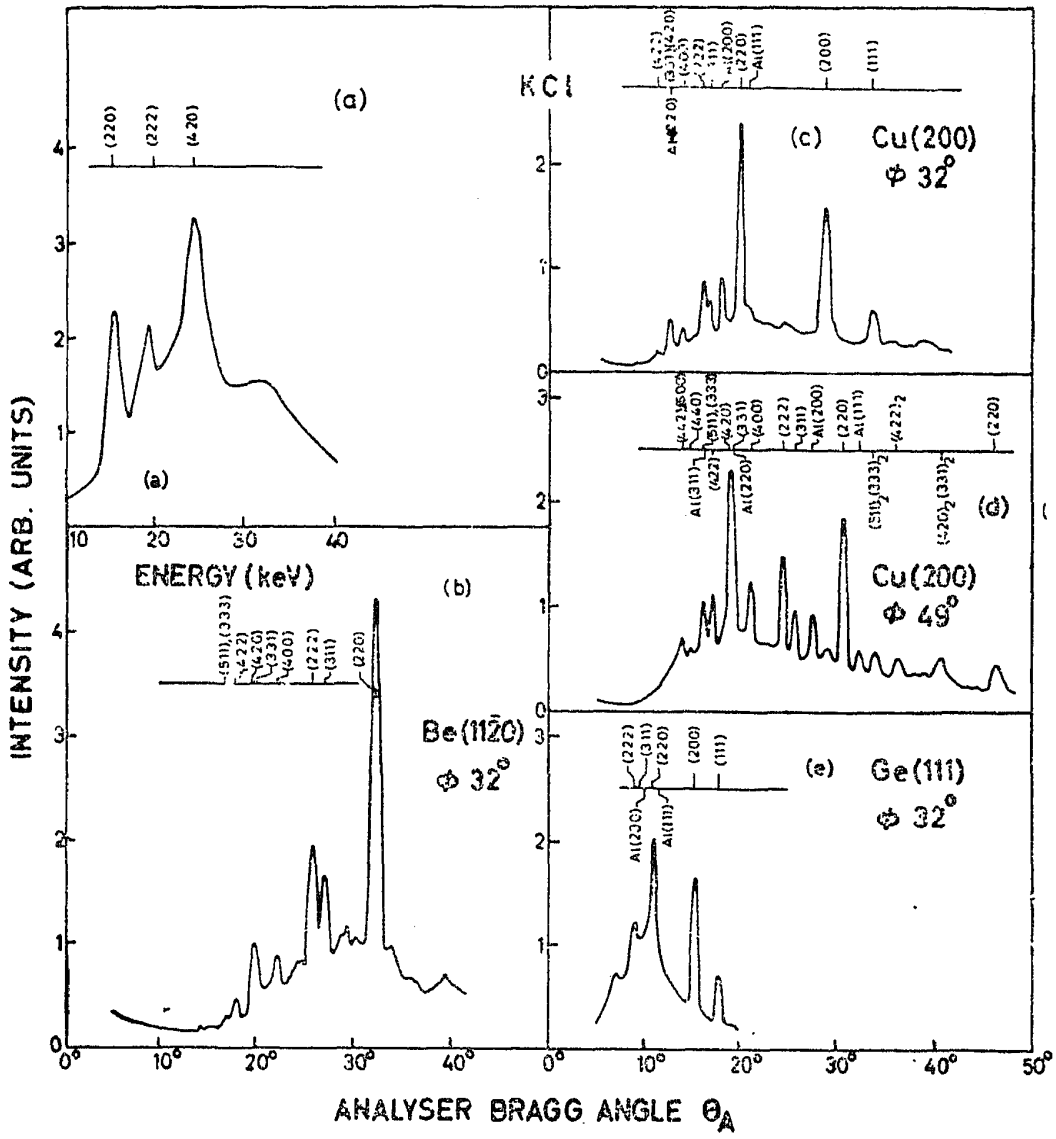

Figure 6. Comparison of results in case of KCl: (*a*) corresponds to data by x-ray energy dispersive technique by Prabudha Banerjee and Paul Chaikit (1971) (*b*) through (*e*) show results obtained by the present technique.

For a particular spectrometer (α_1, α_2, and α_3 fixed), analyser (β_A fixed), and a given scattering angle (θ_0 fixed), $I(hkl)$ can be written simply as

$$I(hkl) = K' \lambda_0^4 \mid F(hkl) \mid^2 i(\lambda_0) R(\lambda_0) \chi(\lambda_0) A(\lambda_0), \tag{33}$$

K' containing now the constant parameters.

Since at any $2\theta_{A_0}$ higher orders of (hkl)s are also acceptable, therefore,

$$I_{\text{total}}(2\theta_{A_0}) = \sum_{\text{all orders}} I(hkl) = \sum_{\text{all orders}} K' \lambda_0^4 \mid F(hkl) \mid^2 \times i(\lambda_0) R(\lambda_0) \chi(\lambda_0) A(\lambda_0). \tag{34}$$

4.1 *Effective spectrum* $I_{\text{eff}}(2\theta_{A_0})$.

The spectrum-weighted analyser-detector efficiency function $I_{\text{eff}}(2\theta_{A_0})$—we shall designate this simply as effective spectrum—is given by

$$I_{\text{eff}}(2\theta_{A_0}) = K' \sum_{\text{all orders}} i(\lambda_0) R(\lambda_0) \chi(\lambda_0) A(\lambda_0). \tag{35}$$

One can measure the effective spectrum by using a hydrogenous sample or any other sample containing nuclei scattering predominantly incoherently. We

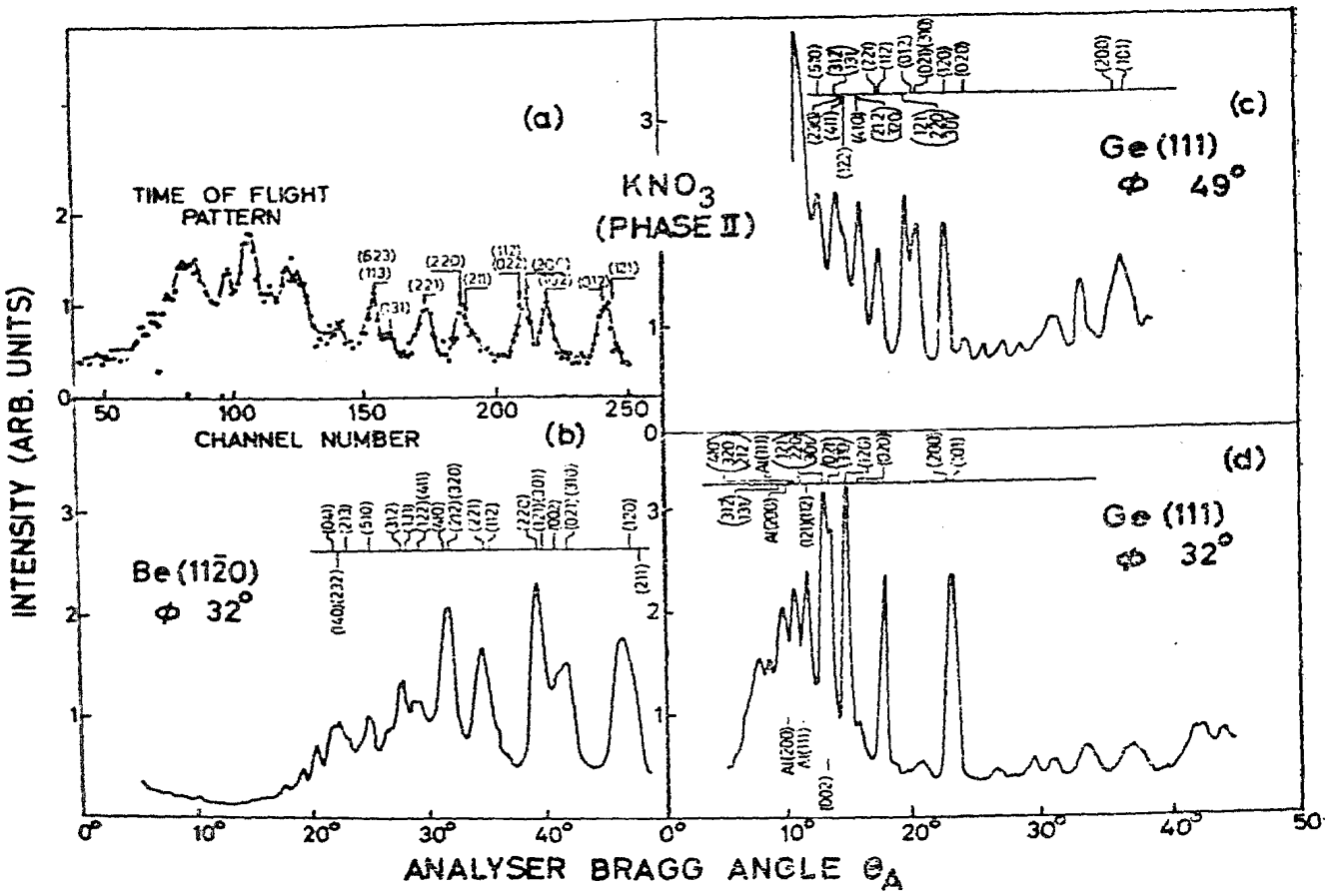

Figure 7. Comparison of results in case of KNO_3: (*a*) Diffraction pattern by TOF method (Brugger *et al* 1965), (*b*) through (*d*) show results by the present technique.

have used samples of perspex and an alloy of $Ti_{0.67}\,Zr_{0.33}$ for this purpose. The effective spectra thus measured for the analysers are shown in figure 4. When absorption is very small as in case of $Ti_{0.67}\;\;Zr_{0.33}$

$$I_{\text{eff}}(2\theta_{A_0}) = K' \sum_{\text{all orders}} i(\lambda_0)\, R(\lambda_0)\, \chi(\lambda_0) \tag{36}$$

One can calculate this using expressions given in the appendix. From the measurements and calculations certain interesting facts emerge:

(*a*) One notices presence of multiple Bragg scattering effects in the spectra predominantly in Cu (200) and Be (11$\bar{2}$0). Ge (111) is almost free from these effects. One should have a precise knowledge of these effects and eliminate these if possible by proper orientation of the analyser. Otherwise reflections from the powder sample which occur at angles where peaks or dips due to multiple Bragg effects are noticeable can be affected as we indeed observe in a few cases.

(*b*) The useful part of the white spectrum is spanned over different ranges of the analyser angle depending on the *d*-spacing of the analyser. The wavelength ranges covered by different analysers are also different.

(*c*) Ge (111) is the most useful analyser because it can be used over a wide wavelength range between $\theta_{A,\min}$ and $\theta_{A,\max}$. In particular if one were to use 'cold' neutrons, Ge (111) would be very profitable. The flat distribution beyond say 20° in case of Ge (111) is mainly due to third order reflection in the analyser.

(*d*) The dashed lines in figure 4 are the results of calculations made using eq. (36) along with eqs (A1), (A2) and (A3). Calculations include contributions from I and II order scattering for Be ($11\bar{2}0$) and Cu (200) analysers and I and III order scattering for Ge (111) (in this case II order is absent) *plus* background. Calculated values are normalised arbitrarily at points shown by ⊗ in each spectrum. At these points II (III in case of Ge (111)) order contribution is negligible. Dotted lines give contributions from I order spectra only without taking into account the background.

(*e*) Agreement between calculated and measured effective spectral shapes may be said to be satisfactory. Departures between calculated and measured spectra may arise from multiple Bragg scattering and extinction effects in the incoherent sample and analyser which we have not taken into account.

The choice of an analyser should depend upon:

(i) nature of the spectrum from the reactor (depending on the actual source, namely, hot, thermal or cold),

(ii) the size of the unit cell of the sample, and

(iii) the scattering angle at the sample.

4.2. *Spectra from samples*

Silicon: Silicon has been studied by TOF diffractometry by Buras *et al* (1964) using both a steady state reactor and a pulsed reactor. At the steady reactor they used a Fermi chopper and found that the resolving power was better at higher speeds of rotation. Peaks corresponding to larger wavelengths say beyond 2 Å were normally absent, due to the cut-off of the chopper. Secondly, they have also observed that the resolving power in TOF technique was comparable to that of the conventional method.

Figure 5 (*a*) shows spectrum from conventional method and figure 5 (*b*) that from TOF method using a pulsed reactor both due to Buras *et al* (1964). Spectra obtained by the present technique employing copper (200) analyser are given in figures 5 (*c*) and 5 (*c'*). One can notice that spectra obtained by the present technique are as good as the spectra from the conventional diffraction technique. However, one has the additional advantage that one can resolve the peaks by going over to larger scattering angles. Secondly, the TOF spectra and spectra obtained by the present technique are also quite similar to each other. In figures 5 (*d*) and 5 (*d'*) we have given spectra using Be ($11\bar{2}0$) and Ge (111) analysers on the θ_A scale to indicate the nature of as-measured spectra. We have analysed the data obtained on the basis of the intensity and resolution expressions discussed in section 3. The appendix gives some details of the calculations, highlighting peculiarities due to the technique. The calculated and measured areas of different (*hkl*) peaks are given in table 1 (*a*). The area under various peaks were measured with respect to a smooth background drawn below the peaks as shown in figure 5 (*c*) by the dashed line. The background arises from neutrons getting scattered from the shielding around the sample and leaking through the collimator onto the analyser and from incoherent scattering from the sample itself. In calculating the integrated intensities we have taken into account second order contributions and a correction factor due to self absorption in the sample. This last factor has made use of absorption coefficient that takes into account variation due to wavelength. We conclude from the comparison of the calculated and measured intensities that

Table 1 (*a*). Integrated intensities for silicon

hkl	Cu analyser $\phi = 32°$		Cu analyser $\phi = 49°$		Be ($11\bar{2}0$) analyser $\phi = 32°$		Ge (111) analyser $\phi = 49°$	
	I_M	I_C	I_M	I_C	I_M	I_C	I_M	I_C
111	523*	308	..	..	..	..	59	42
220	212	259	149	137	290	258	100	100
311	100	100	100	100	100	100	82	71
400	..	9	30	26	7	9	35†	18
331	6	7	39	35	12	5	15	22
422	..	..	21	33	4	2	..	..
511, 333	..	..	11	11	..	..	..	..

* Affected by multiple Bragg Scattering.
† Contaminated by Al (220) peak.

Table 1 (*b*). Half widths for silicon (minutes)

hkl	Cu (200) analyser $\phi = 32°$		Cu (200) analyser $\phi = 49°$		Be ($11\bar{2}0$) analyser $\phi = 32°$		Ge (111) analyser $\phi = 49°$	
	$(\triangle\theta_A)_M$	$(\triangle\theta_A)_C$	$(\triangle\theta_A)_M$	$(\triangle\theta_A)_C$	$(\triangle\theta_A)_M$	$(\triangle\theta_A)_C$	$(\triangle\theta_A)_M$	$(\triangle\theta_A)_C$
111	60	59	..	..	..	..	33	34
220	30	37	34	38	56	57	30	33
311	30	35	30	34	45	48	..	..
400	..	..	30	33	37	40	34	31
331	..	..	37	32	32	38	30	31
422	..	..	21	32	30	36	..	..
511, 333	..	..	30	32	..	..	..	..

the integrated intensities can be accounted for quite well (say to within 15%). However, a few peaks show considerable disagreement [say (111) in column 2]. If we now examine the spectrum with figure 4 we notice that this peak lies close to one of the peaks or valleys in the effective spectrum. In other words, multiple Bragg scattering in the analyser can affect the peak intensities measured by this technique. We mention this so that one is aware of the errors in intensities that may crop up, from this source. It should be possible to overcome the problem by suitable azimuthal orientation of the analyser. We have not attempted this so far. The widths of the peaks are tabulated in table 1 (*b*). Theoretical widths were calculated using the following spectrometer parameters for various collimation divergences: $\alpha_1 = 1°$, $\alpha_2 = 0{\cdot}75°$, $\alpha_3 = 1°$. The mosaic spread of the analysers are assumed to be 15′, 15′ and 3′ for Cu (200), Be ($11\bar{2}0$) and Ge (111) analysers respectively.

Potassium chloride: Figure 6 shows the spectra obtained in the case of KCl. Figure 6 (*a*) indicates the spectrum measured by the x-ray energy dispersive technique (Prabudha Banerjee and Paul Charbit 1971). Figure 6 (*b*) through figure 6 (*e*) corresponds to measurements made by our technique. Table 2 (*a*) gives a comparison of the theoretical and the experimental intensities and table 2 (*b*) the widths. Qualitatively, the features are like those of silicon. It is to be noted that the correction factor for self-absorption in this sample varies considerably compared to that for other samples because of the large absorption cross section of chlorine for neutrons. The (311) reflection is affected by multiple Bragg scattering with both Cu (200) and Be (11$\bar{2}$0) reflection, as well as (422) with Cu (200).

Table 2 (*a*). Integrated intensities for KCl

hkl	Cu (200) analyser $\phi = 32°$		Cu (200) analyser $\phi = 49°$		Be (11$\bar{2}$0) analyser $\phi = 32°$		Ge (111) analyser $\phi = 32°$	
	I_M	I_C	I_M	I_C	I_M	I_C	I_M	I_C
111	31	54	..	..	..	..	38	66
200	115	88	55	..	..	..	100	100
220	100	100	196	171	100	100	96	108
311	15*	50	49*	150	19*	51	..	..
222	23	28	100	100	24	29	..	..
400	7	8	55	54	8	8	..	..
331, 420	17	18	272	229	13	19	..	..
422	5	4	41*	102	3·5	4	..	..
333, 511	..	..	41	47	1·3	1·2	..	..
440	..	..	4	23	..	..	..	..
442, 600, 531	..	..	29	63	..	..	..	..

* Affected by multiple Bragg scattering.

Table 2 (*b*). Half widths for KCl (minutes)

hkl	Cu (200) analyser $\phi = 32°$		Cu (200) analyser $\phi = 49°$		Be (11$\bar{2}$0) analyser $\phi = 32°$		Ge (111) analyser $\phi = 32°$	
	$(\Delta\theta_A)_M$	$(\Delta\theta_A)_C$	$(\Delta\theta_A)_M$	$(\Delta\theta_A)_C$	$(\Delta\theta_A)_M$	$(\Delta\theta_A)_C$	$(\Delta\theta_A)_M$	$(\Delta\theta_A)_C$
111	63	72	..	..	..	..	38	38
200	60	59	71	72	..	..	33	36
220	33	41	43	37	64	68	35	32
311	..	..	37	33	54	55	..	..
222	..	..	36	33	49	53	..	..
400	34	34	33	30	45	45	..	..
422	..	..	32	27	49	38	..	..

Potassium nitrate: Potassium nitrate in phase II at room temperature is the most complex system we have investigated so far by this technique. We chose this sample since we can compare; our data with the TOF data obtained by Brugger *et al* (1965). This study demonstrates the power of the present technique to separate out close lying lines. We feel that it is as good if not superior to the TOF method. There are several peaks in the pattern taken with the Ge (111) analyser which we have not indexed. These arise due to the presence of III order reflection in the analyser. In figure 7 (*c*) and figure 7 (*d*) we have indexed only

Table 3 (*a*). Integrated Intensities for KNO_3

hkl	Be (11$\bar{2}$0) analyser $\phi = 32°$		Ge (111) $\phi = 49°$		Ge (111) $\phi = 32°$	
	I_M	I_C	I_M	I_C	I_M	I_C
101, 200	..	..	142**	60	124	90
020	..	..	18	11	11	12
120	170	168	100	100	100	100
021, 310, 002	133	162	230	253	151	160
220, 121, 301	165	177				
112, 221	100	100	76	79	51	44
410, 212, 320	106	85	86	83	35	37
122, 411	19	8	107	83	27	18
312, 131, 510	28	46				
213, 041, 140, 232	22	18	..	..	..	..
	43	52	..	..	..	..

* Al (200) contamination, **III order contamination.

Table 3 (*b*). Half widths for KNO_3 (minutes)

	Be (11$\bar{2}$0) analyser $\phi = 32°$		Ge (111) $\phi = 49°$		Ge (111) $\phi = 32°$	
	$(\Delta\theta_A)_M$	$(\Delta\theta_A)_C$	$(\Delta\theta_A)_M$	$(\Delta\theta_A)_C$	$(\Delta\theta_A)_M$	$(\Delta\theta_A)_C$
120	120	120	35	34	33	34
510	45	51	..	..	..	..

the first order peaks. Tables 3 (*a*) and 3 (*b*) give a comparison of the experimental and the theoretical intensities and widths.

5. Summary

In the introduction to this paper we have outlined several techniques presently available for neutron diffraction. Amongst them the white beam technique is the most suitable for studying samples in constant geometrical configurations. The Laue technique is applicable only to single crystal studies. One normally resorts to TOF techniques in the study of powder or liquid specimens. These techniques depend on sophisticated and expensive pulsing and electronic devices for getting suitable data.

Section 2 describes the technique developed by us to overcome the shortcomings mentioned above. The technique is based on the principle that the sample can be mounted in the white beam from the beam port of a reactor and at any convenient scattering angle neutrons scattered contain information on diffraction from various (*hkl*) planes in the sample. One can analyse the diffraction intensities due to the different (*hkl*)s using an analyser looking at the specimen. This scheme is simple in mechanical design as there are no pulsing devices and it is less expensive to operate. At the same time the technique meets the requirement of a constant angle geometry. One can therefore adopt this technique for studying samples under high pressure wherein one normally uses a device with one entrance window and one exit window for neutron beams.

The resolution and intensities expected in this method can be calculated using expressions (29) and (31) derived by us in section 3.

We have investigated in sufficient detail the spectra from three different samples namely Si, KCl and KNO_3. The choice of these samples is purely dictated by the fact that one can easily compare the results with those obtained by other white beam techniques. We have used two different scattering angles to examine the effect of contrast and three different analysers namely Cu (200), Be ($11\bar{2}0$) and Ge (111) to illustrate the power and potentiality of the technique. The results are discussed in section 4. In calculating intensities one has to have a good knowledge of the neutron spectrum from the reactor, reflectivity of the analyser, efficiency of the detector, absorption correction in the sample and extinction corrections in the sample and the analyser. We have been able to account for measured intensities to within 15% on a relative scale (except for those cases where multiple Bragg effects viciate the intensities). We believe that the comparison is satisfactory at this stage. Comparison of widths is also satisfactory. There is scope for improvement in data analysis to arrive at better quantitative agreements. Using suitable software available for powder diffraction studies and by properly using extinction corrections one can analyse the data more sophistically. We hope to pursue this in the future.

We believe that the demonstration of this simple technique would encourage one to take up say high pressure diffraction at medium flux reactor centres with reasonable resources.

Acknowledgement

Authors thank P K Iyengar and other colleagues for useful discussions.

Appendix

Calculation of integrated intensities

The effective spectra and integrated intensities for various (*hkl*)s are calculated and tabulated on following basis:

(*a*) The incident spectrum from the reactor is assumed to be a Maxwellian corresponding to a certain moderator temperature. For CIRUS reactor (Moderator temperature $\sim 60°C$) this is given by

$$i(\lambda) = 7{\cdot}7526 \times 10^4 \sqrt{d_A{}^2 E - 0{\cdot}02046}\; E^{5/2}\, e^{-35{\cdot}236E}. \qquad \text{(A1)}$$

The reflectivity for the analyser in reflection and transmission geometry can be assumed to be given by (Rao 1966)

$$R_{\text{reflection}} = \int \frac{\alpha d\xi}{(1+\alpha) + \sqrt{1+2\alpha}\coth A\sqrt{1+2\alpha}}\;;\; A = \frac{\mu(\lambda)\, t}{\sin\theta} \qquad \text{(A2}\_a\text{)}$$

$$R_{\text{transmission}} = \frac{e^{-A}}{2}\int (1 - e^{-2\alpha A})\, d\xi\;;\; A = \frac{\mu(\lambda)\, t}{\cos\theta} \qquad \text{(A2 } b\text{)}$$

where

$$\alpha = \frac{\lambda^3 N^2 F_A{}^2}{(\sqrt{2\pi})\,\mu(\lambda)\,\beta_A}\,\frac{\exp(-\xi^2/2\beta_A{}^2)}{\sin 2\theta_A} \qquad \text{(A2 } c\text{)}$$

with N being the reciprocal of the unit cell volume, $F_A{}^2$, the structure factor for analyser plane; β_A, mosaic spread of the crystal in radians; ξ, the angle between the normal of a mosaic block and normal to crystal surface; $\mu(\lambda)$, wavelength dependent linear absorption coefficient; t, thickness of crystal, and efficiency of our neutron detector is given by

$$\chi(\lambda) = [1 - e^{-0{\cdot}41268/\sqrt{E}}]\, e^{-0{\cdot}03439/\sqrt{E}}, \qquad \text{(A3}$$

E being the energy in eV.

(*b*) We had used Cu (200) in reflection geometry. Ge (111) and Be ($11\bar{2}0$) were used in transmission geometry.

(*c*) The samples used were all powders contained in 6·0 cm high, 1·25 cm diameter (2R) thin aluminium containers. The true absorption cross-section of various elements and other relevant parameters in the samples is given in table 4. In conventional diffraction, one calculates the linear absorption coefficient μ

Table 4.

	Element	True absorption cross-section at 1·08 Å (barns)	N_i (atoms/cc)
I	Si	0·06	$5{\cdot}19\times10^{22}$
II	K	1·2	$1{\cdot}6\times10^{22}$
	Cl	19·2	$1{\cdot}6\times10^{22}$
III	K	1·2	$1{\cdot}26\times10^{22}$
	N	1·1	$1{\cdot}26\times10^{22}$
	O	0·0001	$3{\cdot}76\times10^{22}$

equal to $\sum_i N_i\sigma_i$; N_i, the number of atoms of species i per cc and σ_i the true absorption cross-section of the species i and estimates the absorption correction A^* [see *International Tables of Crystallography* Vol. II, 295 (1959)] as a function of scattering angle using the same μR for a given cylindrical sample of diameter $2R$. In the present technique, since the scattering angle is fixed but the wavelength is variable, we have evaluated μ as a function of wavelength. We have made use of the fact that σ_i varies inversely as velocity of the neutron (or directly as the wavelength of the neutron). We have used table 5.3.5B of *International Tables of Crystallography* Vol. II to obtain A^* as a function of θ_A for a fixed scattering angle.

Figure 8 shows the variation of A^* as a function of θ_A for KCl with the different analysers for two scattering angles $\phi = 32°$ and $49°$ in the lower part of the figure. One notices that the variation of A^* is as much as a factor of four for a scan of nearly $50°$ in θ_A whereas in conventional diffraction using say 1·08 Å, the variation of A^* would have been a factor of 1·05 over a scan of say $90°$ in ϕ. The upper part of the same figure shows variation of A^* for KNO_3 for the three analysers (Note the change in scale for the ordinates). There is negligible difference in A^* between the two scattering angles for any analyser in this case. Because of the very low absorption cross-section for silicon, $A^* \simeq 1{\cdot}0$ for all analysers at all θ_A and all scattering angles. We have taken into account A^* in quoting the calculated corrected integrated intensities in tables 1, 2, and 3.

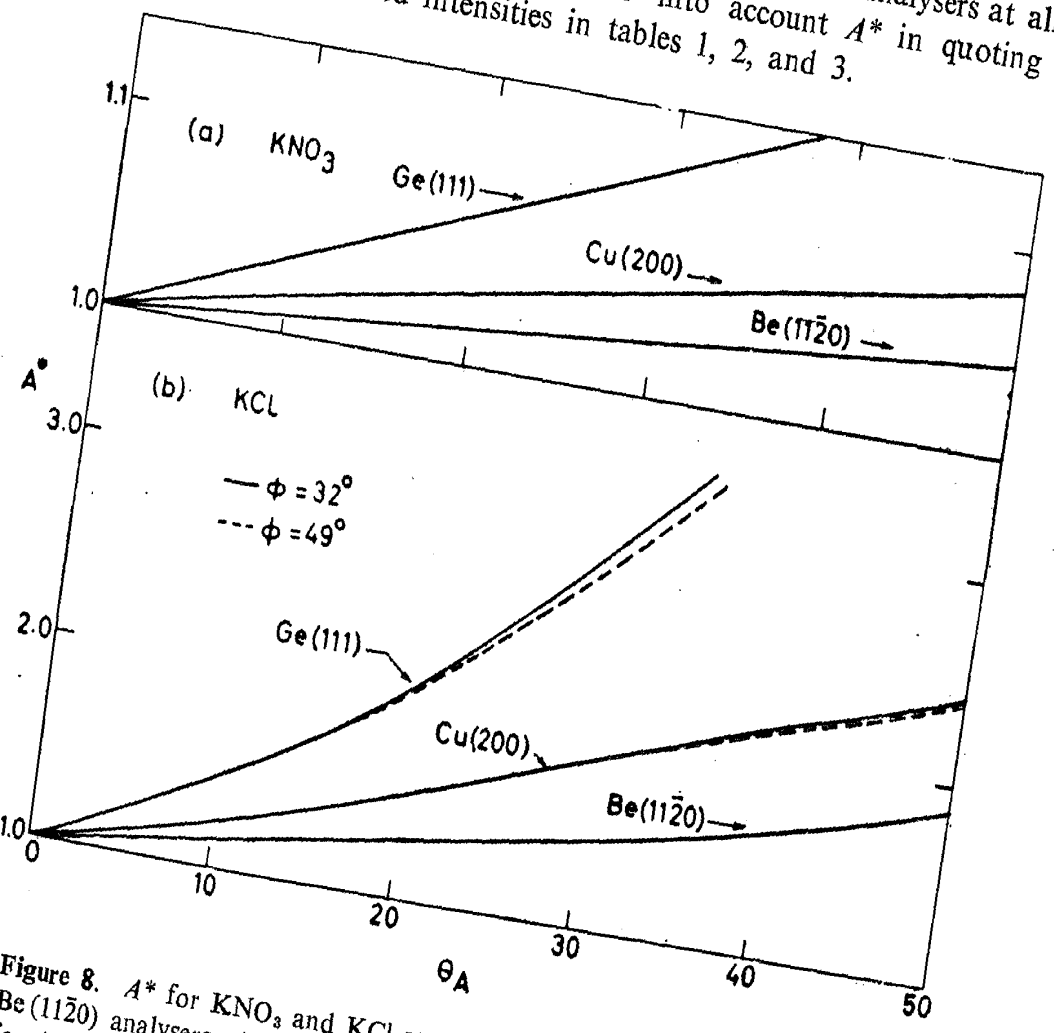

Figure 8. A^* for KNO_3 and KCl as a function of θ_A for Ge (111), Cu (200) and Be (11$\bar{2}$0) analysers. In case of KNO_3, there is negligible difference between A^* for $\phi = 32°$ and $\phi = 49°$. In case of KCl, the difference is larger and the full lines and dashed lines indicate A^* for $\phi = 32°$ and $\phi = 49°$ respectively.

(*e*) The experimentally measured integrated intensity $I_M(hkl)$ is obtained as follows: A smooth background is drawn below the diffraction peaks as shown by the dashed line in figure 5(*c*). The area of the peak above this background is measured and this corresponds to $I_M(hkl)$. Errors in $I_M(hkl)$ arise due to uncertainty in estimating the background particularly for weak peaks.

(*f*) The values quoted in tables 1, 2, and 3 for both $I_C(hkl)$ and $I_M(hkl)$ have been normalised to $I_C(HKL)$ and $I_M(HKL)$ where (HKL) is an intense diffraction peak containing negligible II order or higher order contribution. $I_C(HKL)$ and $I_M(HKL)$ are quoted as 100 in the tables and the other values are given with respect to this number.

References

Albritton L M and Malgrave J L 1972 *High Temp. High Pressures* **4** 13

Brugger R M 1965 *USAEC Report IDO* 17106

Brugger R M, Bennion R B, Worlton T G and Patterson E R 1965 *USAEC Report IDO* 17170

Brugger R M, Bennion, R B, Worlton T G and Myers W R 1969 *Trans. Amer. Cryst. Assn.* **5** 141

Buras B 1963 *Nukleonika* **8** 1975

Buras B, Leceijewicz J, Nitc W, Sosnowska I, Sosnowski J and Shapiro F 1964 *Nukleonika* **9** 523

Buras B, Giebultowicz T, Minor W and Rajka A 1970 *Nucl. Instrum. Methods* **77** 13

Buras B, Lebecn B, Kofoed W and Backstrom G 1973 *Riso Report* 300 44

Buras B, *RCN Report* 234, 307 1975 Proc. Neutron Diffraction Conf. Petten

Caglioti G, Paoletti A and Ricci F P 1958 *Nucl. Instrum. Methods* **3** 228

Cole H H 1970 *J. Appl. Cryst.* **3** 405

Colwell J F, Miller P H and Whittemore W L 1968 *Neutron Inelastic Scattering* (International Atomic Energy Agency, Vienna) Vol. II 429

Gieson B C and Gordon G E 1968 *Science* **159** 973

Gompf F, Reichardt W, Glasser W and Beckurts K H 1968 *Neutron Inelastic Scattering* (International Atomic Energy Agency, Vienna Vol. II 417

Hubbard C R, Quicksaal C O and Jacobson R A 1972 *Acta Cryst.* **A28** 236

Hubbard C R, Quicksaal C O and Jacobson R A 1974 *Acta Cryst.* **B30** 2619

Iyengar P K 1965 *Symp. on Inelastic Scattering of Neutrons by Condensed Systems* (Brookhaven National Laboratory, USA) BNL 940 p. 179

Khadake R G 1973 *The Use of a Solid State Radiation Detector in x-ray Diffraction Experiments* M.Sc. Thesis (unpublished)

Prabudha Banerjee and Paul Charbit 1971 *Seimens Z.* **45** 8

Rao K R 1966 *AEET Report* 259

Rao K R 1968 *Structure and Dynamics of Liquids by Neutron Scattering* Ph.D. Thesis—unpublished

Sailor V L, Foote Jr.L, London H H and Wood R W 1956 *Rev. Sci. Instrum.* **27** 26